

Object-Centric Diffusion for Efficient Video Editing

Kumara Kahatapitiya* Adil Karjauv Davide Abati Fatih Porikli
Yuki M. Asano Amirhossein Habibian

Qualcomm AI Research[†]

{kkahatap, akarjauv, dabati, fporikli, ahabibian, asano}@qti.qualcomm.com

Abstract

Diffusion-based video editing have reached impressive quality and can transform either the global style, local structure, and attributes of given video inputs, following textual edit prompts. However, such solutions typically incur heavy memory and computational costs to generate temporally-coherent frames, either in the form of diffusion inversion and/or cross-frame attention. In this paper, we conduct an analysis of such inefficiencies, and suggest simple yet effective modifications that allow significant speed-ups whilst maintaining quality. Moreover, we introduce Object-Centric Diffusion, coined as OCD, to further reduce latency by allocating computations more towards foreground edited regions that are arguably more important for perceptual quality. We achieve this by two novel proposals: i) Object-Centric Sampling, decoupling the diffusion steps spent on salient regions or background, allocating most of the model capacity to the former; and ii) Object-Centric 3D Token Merging, which reduces cost of cross-frame attention by fusing redundant tokens in unimportant background regions. Both techniques are readily applicable to a given video editing model without retraining, and can drastically reduce its memory and computational cost. We evaluate our proposals on inversion-based and control-signal-based editing pipelines, and show a latency reduction up to 10× for a comparable synthesis quality.

1. Introduction

Diffusion models [12, 43] stand as the fundamental pillar of contemporary generative AI approaches [14, 19, 38]. Their success primarily stems from their unparalleled diversity and synthesis quality, surpassing the capabilities of the earlier versions of generative models [9, 20]. On top of that, recent methods such as Latent Diffusion Models (LDMs) [38] exhibit scalability to high-resolution inputs and adaptability to different domains without requiring retraining or finetuning, especially when trained on large-scale datasets [41].

*Work completed during internship at Qualcomm Technologies, Inc.

[†]Qualcomm AI Research is an initiative of Qualcomm Technologies, Inc.

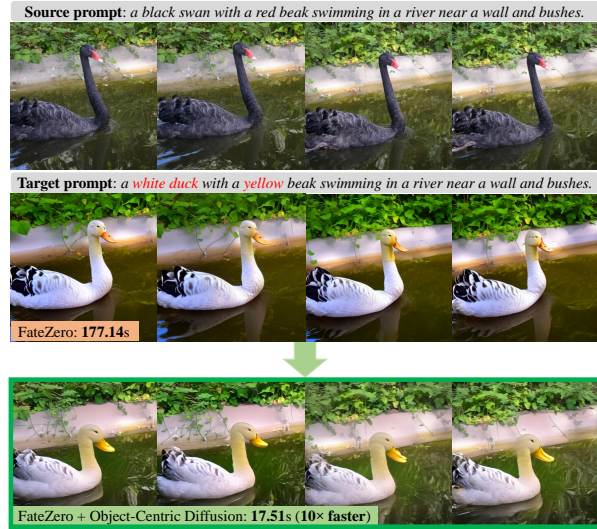


Figure 1. **OCD speeds up video editing.** We show exemplar editing results of FateZero [33] with and without our OCD optimizations. When including our techniques, the editing is 10× faster than the baseline with similar generation quality.

These traits catalyzed impactful adaptations of pretrained LDMs across a spectrum of applications, including text-guided image generation [38], editing [1], inpainting [38], as well as video generation [2] and editing [33, 46, 49].

Nevertheless, diffusion models come with various trade-offs. One immediate drawback is their inefficiency due to the sampling process, which involves iterating a denoising neural network across numerous diffusion steps. Despite the availability of techniques like step distillation [29, 40] and accelerated samplers [26, 27, 43] that expedite image synthesis, efficient sampling solutions for video generation are still lacking. Besides, special attention must be paid to maintaining temporal coherency among frames when creating or modifying a video. Otherwise, it may result in flickering artifacts or a complete lack of correlation between frames. To tackle this challenge, approaches like diffusion inversion [33, 43] and cross-frame self-attention [33, 49] have been introduced, but all at the cost of significantly increasing the computational load.

This paper centers on video editing models and presents

novel solutions to enhance their efficiency. We first examine the current video editing frameworks, identifying the key elements that impede their effectiveness. These encompass memory overheads, such as those associated with attention-based guidance from diffusion inversion, as well as computational bottlenecks, including excessive cross-frame attention and an unnecessarily high number of sampling steps. We show that significant improvements can be achieved by adopting off-the-shelf optimizations namely efficient samplers and leveraging token reduction techniques in attention layers such as token merging (ToMe) [3, 4].

Additionally, we argue that during video editing, users may be particularly sensitive to the quality of edited foreground objects compared to any potential degradations in the background regions. Consequently, we propose two new and efficient techniques that harness this object-centric aspect of editing applications. Our first solution, *Object-Centric Sampling*, involves separating the diffusion process between edited objects and background regions. This strategy enables the model to focus the majority of its diffusion steps on the foreground areas. Consequently, it can generate unedited regions with considerably fewer steps, all while ensuring faithful reconstructions in all areas. With our second solution, *Object-Centric 3D ToMe*, we incentivise each token reduction layer to merge more tokens within less crucial background areas and exploit temporal redundancies that are abundant in videos. The combination of such techniques, coined Object-Centric Diffusion (OCD), can seamlessly be applied to any video editing method without re-training or finetuning.

As we demonstrate in extensive experiments, the combined implementation of these object-centric solutions enhances the quality of video editing in both salient foreground object and background, while considerably reducing the overall generation cost. We apply our proposed solutions to inversion-based and ControlNet-based video editing models, speeding them up by a factor of $10\times$ and $6\times$ respectively while also decreasing memory consumption up to $17\times$ for a comparable quality (see Fig. 1).

We summarize our contributions as follows:

- We analyze the cost and inefficiencies of recent inversion-based video editing methods, and suggest simple ways to considerably speed them up.
- We introduce Object-Centric Sampling, which separates diffusion sampling for the edited objects and background areas, limiting most denoising steps to the former to improve efficiency.
- We introduce Object-Centric 3D ToMe, which reduces number of cross-frame attention tokens by fusing redundant ones predominantly in background regions.
- We showcase the effectiveness of OCD by optimizing two recent video editing models, obtaining very fast editing speed without compromising fidelity.

2. Related work

Text-based Video Generation & Editing There has been a surge in text-to-video generation methods using diffusion models. The early works inflate the 2D image generation architectures to 3D by replacing most operations, *i.e.* convolutions and transformers, with their spatio-temporal 3D counterparts [13, 15, 16, 42, 50]. Despite their high temporal consistency, these substantial model modifications requires extensive model training on large collection of captioned videos.

To avoid extensive model trainings, recent works adopts off-the-shelf image generation models for video editing in one-shot and zero-shot settings. One-shot methods rely on test-time model adaption on the editing sample which is still too slow for real-time applications [6, 46]. Zero-shot methods integrate training-free techniques into the image generation models to ensure temporal consistency across frames [8, 17, 24, 33, 49] most commonly by: *i)* providing strong structural conditioning from the input video [5, 7, 49] inspired by ControlNet [48]. *ii)* injecting the activations and attention maps extracted by diffusion inversion [43, 44] of the input video into the generation [8, 33]. *iii)* replacing the self-attention operations in the denoising UNet with cross-attention where the key and value tokens are being extracted from neighboring frames [33, 46, 49]. Introducing cross-frame attention greatly increases the temporal consistency especially when using more neighboring frames [49]. Despite their effectiveness, all these temporal solutions come with additional computational cost which is under explored in the literature.

Efficient Diffusion Models Due to their sequential sampling, diffusion models are computationally very expensive. Several studies analyze the denoising U-Net architecture to enhance its runtime efficiency, achieved either through model distillation [18] or by eliminating redundant modules [23]. Other ways to obtain efficiency gains include enhanced noise schedulers [26, 27] and step distillation techniques [23, 29, 40]. The most relevant to our work is the Token Merging technique presented in [4] that demonstrated advantages for image generation [3]. Although very proficient, we observe it does not readily work when deployed in video editing settings. For this reason, we optimize this technique for the task at hand, such that it exploits redundancy of tokens across frames and directing its token fusing towards background regions. Similar to our object centric sampling, [22] aims for an efficient editing by skipping the computations on unedited regions for interactive image editing: the user interactively edits different regions of an image. They cache the representation during generations to use it for unedited regions in future edits. Instead of caching the features, our proposed object centric sampling is not limited to interactive editing applications.

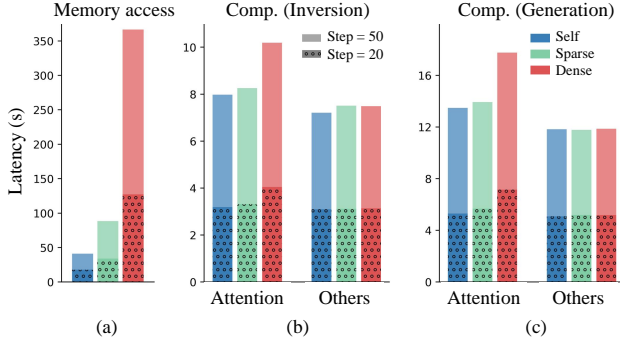


Figure 2. **Latency analysis** of video editing models. At various diffusion steps, latency is dominated by memory access operations. Among pure computations, attention alone is the bottleneck, especially when using dense cross-frame interactions. As attention is the main responsible for most of the memory overhead, we hypothesize that reducing the number of its tokens have a significant impact on latency.

3. Efficiency Bottlenecks

To investigate the main latency bottlenecks in video editing pipelines, we run a benchmark analysis on a representative pipeline, derived from FateZero [33]. More specifically, in this case-study we are primarily interested in the role of components such as diffusion inversion and cross-frame attention, as these techniques are crucial for the task and ubiquitous in literature [8, 33, 46, 49]. To study the impact of such components, we collect their latency by probing the model using DeepSpeed [30] while varying (1) the number of diffusion steps (50→20), and (2) the span of cross-frame attention, *i.e.* self (1-frame), sparse (2-frames) or dense (8-frames). Based on the latency measurements aggregated over relevant groups of operations as reported in Fig. 2 we make the following observations:

Observation 1. As demonstrated in Fig. 2 (a), inversion-based pipelines are susceptible to memory operations. Not only that the latency due to memory access dominates the overall latency in all the tested settings, but it also scales exponentially with the span (*i.e.*, #frames) of cross-frame attention.

Observation 2. When ruling out memory and considering computations only, as in Fig. 2 (b) and Fig. 2 (c), we appreciate that attention-related operations are as expensive as (or often more) than all other network operations combined (*i.e.* convolutions, normalizations, MLPs etc.) This latter finding is consistent both during inversion and generation phase.

Observation 3. Using more-powerful cross-frame attentions (*i.e.*, dense) that increases the temporal stability of generations [49], comes at a high latency cost as observed in Fig. 2 (b) and Fig. 2 (c).

3.1. Off-the-shelf acceleration

We explore whether the solutions available for image generation mitigate the key computational bottlenecks observed for video editing. More specifically, we study whether token merging [4], as an effective strategy to improve the attention cost for image generation [3], reduces the high memory and computational cost of video editing. Moreover, given the linear relation between the number of diffusion steps and memory costs of inversion-based editing to store the attention maps and activations [8, 33, 44, 46], we explore how using faster noise schedulers improves the video editing efficiency. In the followings, we describe how the off-the-shelf accelerations are adopted for video editing:

Faster self-attention Aiming to speed-up attention operations, we utilize ToMe [3, 4] to merge redundant tokens. More specifically, ToMe first splits the input self-attention tokens into source (*src*) and destination (*dst*) sets. Then, the similarity between the source token \mathbf{x}_i and the destination token \mathbf{x}_j is computed based on normalized cosine similarity as follows:

$$\text{Sim}(\mathbf{x}_i, \mathbf{x}_j) = \frac{1}{2} \left[\frac{\mathbf{x}_i \cdot \mathbf{x}_j}{\|\mathbf{x}_i\| \|\mathbf{x}_j\|} + 1 \right]. \quad (1)$$

Finally, the top $r\%$ similarities are selected, and source tokens are piggybacked into the corresponding destination tokens by means of average pooling. This process reduces successive operations by removing merged tokens, as only destination and unmerged-source tokens (*unm*) are forwarded, at the cost of a slight information loss.

In our first round of experimentation, we observed the potential of ToMe in speeding up video editing, as a simple reduction of $1/16$ in key-value tokens reduces the model latency by a factor of $4\times$. Nevertheless, its naive application completely breaks generation quality, as testified in Fig. 3 (d). However, we could restore an outstanding generation quality by applying two simple yet crucial tricks. Specifically, we *i*) pair the token locations (both *dst* and *unm*), for the same network layer and diffusion timestep, between inversion and generation (see ToMe-paired Fig. 3(e)), and *ii*) we resample the destination token locations for every frame (Fig. 3 (f)). We refer the reader to the supplementary material for more details about these ToMe optimizations.

Faster noise scheduler Although we observe that the commonly-used DDIM scheduler [43] suffers considerable quality degradation when reducing the number of diffusion steps (without any finetuning), we notice this is not the case with a more modern DPM++ [27], that can operate with as few as 20 iterations. As illustrated in the example reported in Fig. 3 (c), this replacement does not affect the quality of the editing, yet it impacts the generation latency tremendously.



Figure 3. **Off-the-shelf accelerations:** We obtain significant latency gains by adopting off-the-shelf techniques with a few non-trivial modifications. First, we replace the (b) default DDIM [43] sampler with (c) DPM++ [26, 27], which allows us to reduce sampling steps from 50→20 without heavy degradation. Next, apply ToMe to reduce memory and computational overhead resulting from attention modules. Despite the speed-up, generations significantly worsen (d). As remedies, we implement (e) pairing of token locations (both destination and unmerged-source) between inversion and generation, and (f) resampling of destination token locations for every frame, regaining the quality. Altogether, coin the result of these optimizations *Optimized-FateZero*. Best viewed zoomed-in.

In the remainder of the paper, we refer to models optimized with these off-the-shelf accelerations as *optimized*, and will serve as strong baselines to our proposed Object Centric Diffusion.

4. Object-Centric Diffusion

Although off-the-shelf optimizations can notably improve latency, further reductions can be achieved by exploiting the object-centric nature of video editing tasks. As such, following our key assumption regarding the significance of foreground objects for many video editing applications, we propose two add-ons for diffusion models to channel their computational capacity towards foreground regions: *i*) a diffusion sampling process that performs more sampling steps around the foreground regions as described in Sec. 4.1, and *ii*) a token reduction technique to minimize the background tokens, complemented by an effective spatiotemporal merging strategy outlined in Sec. 4.2. For both these contributions, we assume we have a foreground mask m , highlighting in every frame the locations of objects to be edited. Such mask can be obtained by means of a segmentation model [21], visual saliency [34, 47] or by cross-attention with text-prompts.

4.1. Object-Centric Sampling

The process of sampling in diffusion models entails gradually transitioning from the initial noise $\mathbf{z}_T \sim \mathcal{N}$ to the sample derived from the real data distribution \mathbf{z}_0 through denoising steps $p(\mathbf{z}_{t-1}|\mathbf{z}_t)$. Each denoising step involves running a computationally-heavy denoising UNet [39], where high-quality generations demand a large number of sampling steps. The state-of-the-art methods rely on efficient noise schedulers [26, 27] and step distillation [23, 25, 40] to minimize the number of required sampling steps.

Complementing the above, we introduce an efficient object-centric diffusion sampling technique tailored for editing

tasks, prioritizing high-quality generation specifically in designated foreground regions.

As described in Algorithm 1, we divide the latent variable \mathbf{z}_T according to the foreground mask m (e.g. a segmentation mask commonly available in video datasets or from a detector) into foreground and background latents denoted by \mathbf{z}_T^f and \mathbf{z}_T^b . Instead of running the same number of sampling steps for the foreground and background regions, we reduce the sampling steps on the background based on the hyperparameter φ . To avoid inconsistent generation across foreground and background, we merge the denoised latents at a certain sampling step specified by the hyperparameter γ . We empirically observed that allocating $\approx 25\%$ of the sampling steps to this blending stage is usually sufficient to generate spatially and temporally consistent frames.

We note that for localized editing tasks, e.g. shape and attribute manipulations of objects, the background sampling stage can be completely skipped, which results in even faster generation and higher fidelity reconstruction of background regions, as demonstrated in Fig. 7.

Given potentially irregular shape of the foreground masks, sampling of foreground and background regions involves running the UNet on sparse inputs. This requires using efficient sparse convolution and transformers as implemented in [10, 22, 37, 45]. To avoid using custom sparse operations in our implementation, we pad the mask to have a rectangular shape then extract a full crop around the foreground object, and use dense computations to denoise this crop. This simple implementation comes at the cost of not fully-utilizing the sparsity of foreground objects, that can be further improved by integrating the sparse engine implementation from [22]. As demonstrated in our experiments, a naive implementation still results in significant speed-ups, especially for smaller foreground regions.

Algorithm 1 Object-Centric Sampling

Require: Number of training steps T ▷ Default: 1000

Require: Number of inference steps N ▷ Default: 20

Require: Blending steps ratio $\gamma \in [0, 1]$ ▷ Default: 0.25

Require: Background acceleration rate $\varphi > 1$
Require: Foreground mask $m \in \{0, 1\}^{H \times W}$
 $\Delta T \leftarrow T/N$ ▷ Calculate step size

 $T_b \leftarrow \gamma * T$ ▷ Calculate step to start blending

// Split foreground and background latents
 $\mathbf{z}_T \sim \mathcal{N}(0, I)$
 $\mathbf{z}_T^f \leftarrow \text{gather}(\mathbf{z}_T, m)$
 $\mathbf{z}_T^b \leftarrow \text{gather}(\mathbf{z}_T, 1 - m)$
// Sampling the foreground latents at normal rate
for $t = T$; $t > T_b$; $t = t - \Delta T$ **do**
 $\mathbf{z}_{t-1}^f \sim p(\mathbf{z}_{t-1}^f | \mathbf{z}_t^f)$
end for
// Sampling the background latents at faster rate
for $t = T$; $t > T_b$; $t = t - \varphi * \Delta T$ **do**
 $\mathbf{z}_{t-1}^b \sim p(\mathbf{z}_{t-1}^b | \mathbf{z}_t^b)$
end for
// Merge then continue sampling
 $\mathbf{z}_t \leftarrow \text{scatter}(\mathbf{z}_t^f, \mathbf{z}_t^b)$
for $t = T_b$; $t > 0$; $t = t - \Delta T$ **do**
 $\mathbf{z}_{t-1} \sim p(\mathbf{z}_{t-1} | \mathbf{z}_t)$
end for

4.2. Object-Centric 3D Token Merging

We further introduce an effective technique that promotes token merging in background areas while discouraging information loss in representations of foreground objects. More specifically, when applying ToMe, we associate each source token \mathbf{x}_i a binary value $m_i \in \{0, 1\}$, obtained by aligning foreground masks to latent resolution, that specifies whether it belongs to the foreground region. Then, we simply account for m_i in computing similarity between the source token \mathbf{x}_i and the destination token \mathbf{x}_j , as follows:

$$\eta\text{-Sim}(\mathbf{x}_i, \mathbf{x}_j, m_i) = \begin{cases} \text{Sim}(\mathbf{x}_i, \mathbf{x}_j) & \text{if } m_i = 0; \\ \eta \cdot \text{Sim}(\mathbf{x}_i, \mathbf{x}_j) & \text{if } m_i = 1, \end{cases}$$

where $\eta \in [0, 1]$ is a user-defined weighting factor such that $\eta = 1$ corresponds to the original ToMe. By reducing the value of η we reduce similarities of source tokens corresponding to edited objects, and therefore reducing their probability of being merged into destination tokens. The behavior of the weighted similarity metric $\eta\text{-Sim}$ can be appreciated in Fig. 4. As shown, the unmerged tokens (in blue) tend to stay more and more on the edited object while the merged tokens fall in background areas as η decreases, although destination tokens are still sampled dis-

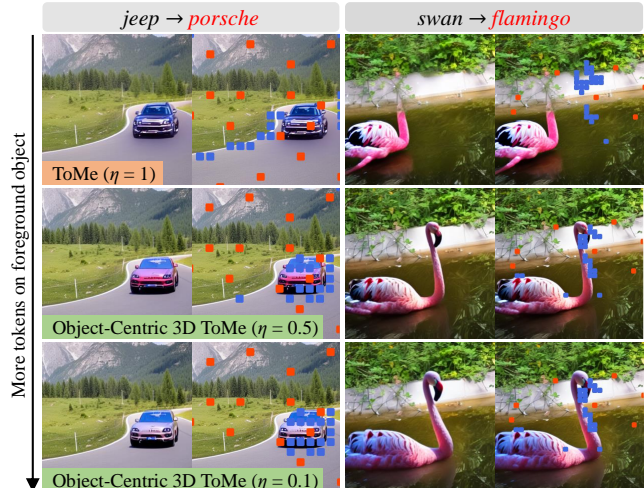


Figure 4. **Object-Centric 3D Token Merging:** By artificially down-weighting the similarities of source tokens of foreground objects, we accumulate in their locations tokens that are left unmerged (in blue). Destination tokens (in red) are still sampled randomly within a grid, preserving some background information. Merged source tokens (not represented for avoiding cluttering) will come from the background.

tributed across spatiotemporal volume.

Merging in 3D Diffusion-based video editing heavily relies on cross-frame attention operations to increase the temporal-consistency in generated frames [49]. Given its quadratic cost, this layer becomes the main computational bottleneck especially when increasing the number of frames it involves (Sec. 3). The standard ToMe only merges tokens in the spatial dimension. This is sub-optimal as it does not allow merging along the temporal dimension, which is the main source of redundancy for video. As a remedy, we apply ToMe *within spatiotemporal volumes*. Besides taking advantage of temporal redundancy, this strategy allows greater flexibility in choosing how to trade-off merging spatial vs. temporal information, by simply varying the size of the volumes.

5. Experiments

We apply our proposed strategy in the context of two families of video editing models. Specifically, we look into inversion-based video editing, where we rely on FateZero [33] as base model, and control-signal-based architectures, for which we optimize a ControlVideo [49] baseline. To provide fair comparisons in each setting, we rely on checkpoints and configurations provided by the corresponding authors. We evaluate each model using a benchmark of DAVIS [32] video sequences and edit prompts utilized in the original baseline methods. We refer the reader to supplementary materials for more-detailed setup.

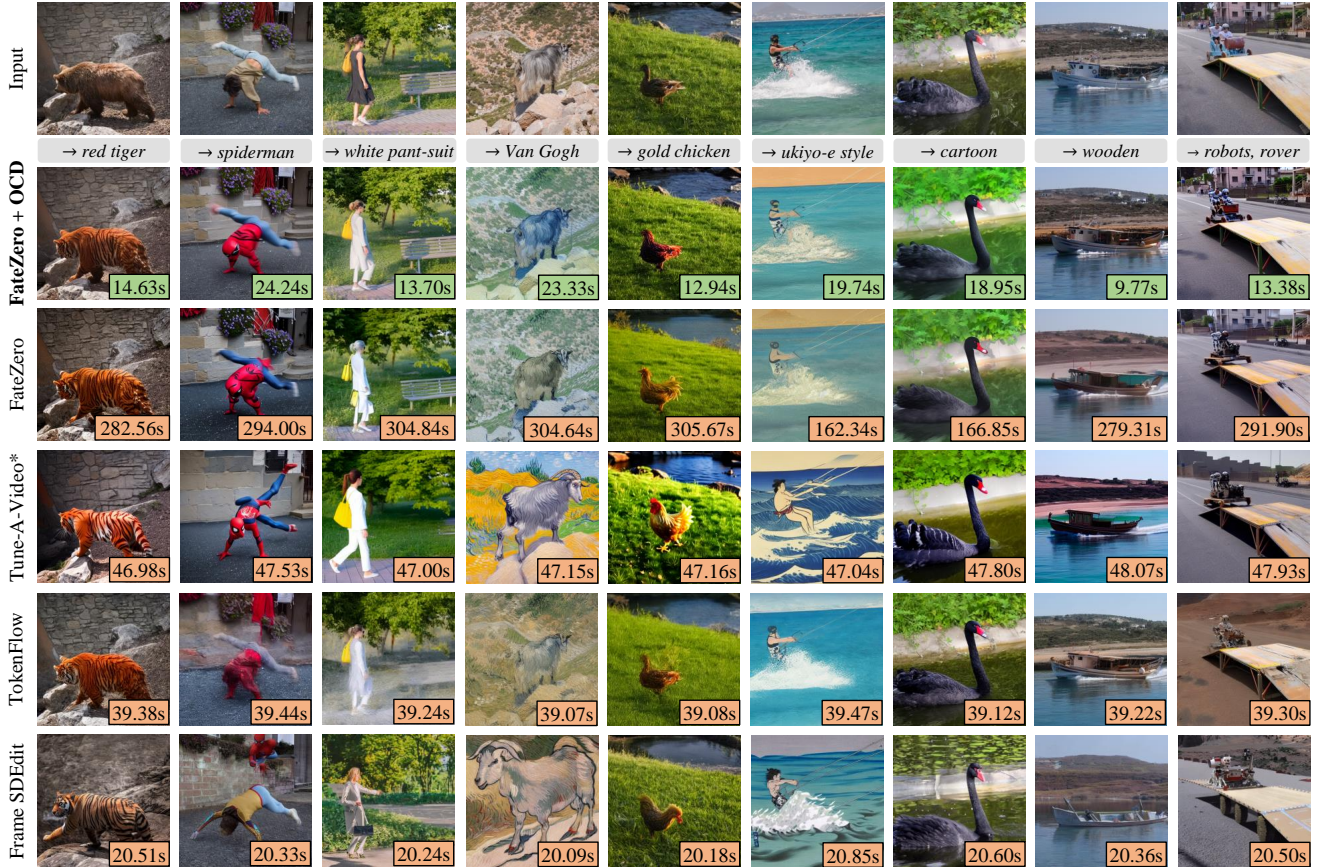


Figure 5. **Qualitative comparison with the state-of-the-art:** We present video frames edited using our method, in comparison with outputs from FateZero [33], Tune-A-Video [46], TokenFlow [8] and SDEdit [28]. Here, Tune-A-Video [46] is always 1-shot finetuned on each sequence (denoted with *), whereas the other methods are zero-shot. Our method gives significantly-faster generations over the baseline we build on-top of (i.e., FateZero [33]), without sacrificing quality. It is also more efficient compared to other state-of-the-art video baselines. Best viewed zoomed-in.

As common in the literature and because we target zero-shot video editing, we optimize some of the hyperparameters (e.g. blending steps ratio γ , similarity re-weighting factor η) per-sequence for FateZero. For ControlVideo, we adopt the original hyperparameters reported in the paper.

Evaluation metrics: For evaluating editing quality, we rely on fidelity metrics such as Temporal-Consistency of CLIP embeddings (Tem-con) and average CLIP-score aggregated over all sequence-prompt pairs. To report latency, we measure the average wall-clock time to edit a video on a single V100 GPU.

5.1. Inversion-based Video Editing

Benchmark details Following the benchmark in [33], we report a quantitative comparison based on 9 sequence-prompt pairs (7 from DAVIS and 2 in-the-wild). We include inversion-based video models such as Tune-A-Video + DDIM [43, 46] and TokenFlow + PnP [8, 44] in the

evaluation. We also show results for a frame-based editing model, namely Framewise Null + p2p [11, 31]. We finally report results of the optimized baseline with fast sampling and ToMe (as discussed in Sec. 3.1 applied on top of FateZero), i.e., Optimized-FateZero.

Main results A qualitative comparison of state-of-the-art models is reported in Fig. 5, where we observe how our model enjoys the lowest latency, while ensuring a comparable editing quality. We report fidelity and latency measurements in Tab. 1, where our model achieves remarkable latency gains of $10\times$ w.r.t. FateZero, and proves significantly faster than other state-of-the-art methods with comparable fidelity metrics. Although Optimized-FateZero is also a plausible model, we observe via visual assessment that its editing quality can be suboptimal, even though certain artifacts in generation might not be captured in CLIP fidelity metrics (for a clear example of this, please see the ablation in Fig. 7).

Model	Tem-con \uparrow	Cl-score \uparrow	Latency (s) \downarrow	
			Inversion	Generation
Framewise Null + p2p [11, 31]	0.896	0.318	1210.60	130.24
Tune-A-Video + DDIM [43, 46]	0.970	0.335	16.50	33.09
TokenFlow + PnP [8, 44]	0.970	0.327	10.56	28.54
FateZero [33]	0.961	0.344	135.80	41.34
Optimized-FateZero	0.966	0.334	9.54	10.14
+ Object-Centric Diffusion	0.967	0.331	8.22	9.29

Table 1. **Quantitative comparison with inversion-based video editing pipelines:** Here we consider FateZero [33] benchmark setting. We report CLIP metrics of fidelity (Temporal-consistency, CLIP-score) and latency. Our method achieves significant speed-up compared to the baseline and other the state-of-the-art methods (either video or framewise), without sacrificing generation quality.

Model	Tem-con \uparrow	Cl-score \uparrow	Latency (s) \downarrow
Text2Video-Zero [17]	0.960	0.317	23.46
ControlVideo [49]	0.972	0.318	152.64
Optimized-ControlVideo	0.978	0.314	31.12
+ Object-Centric Diffusion	0.977	0.313	25.21

Table 2. **Quantitative comparison with ControlNet-based video editing pipelines:** we report CLIP metrics of fidelity (Temporal-consistency, CLIP-score) and latency computed on the ControlVideo [49] benchmark setting with Depth conditioning. With comparable generation quality, our method achieves a significant 6 \times speed-up compared to the baseline.

5.2. ControlNet-based Video Editing

Benchmark details We follow the evaluation benchmark presented in [49] for evaluating ControlNet-based algorithms. The comparison is again based on sequences from DAVIS, and comprises 125 sequence-prompt pairs (detailed in the supplement), for which, per-frame depth maps are extracted using [36] and used as control signal. Besides our main baseline ControlVideo [49], we include Text2Video-Zero [17] in the comparisons. Once again, we will also report the performances of off-the-shelf optimizations as Optimized-ControlVideo.

Main results Fig. 6 illustrates some visual examples. As the figure shows, our proposal shows a significant 6 \times speed-up over the baseline, obtaining a comparable generation quality. We also report a quantitative comparison of ControlNet-based methods in Tab. 2, observing similar outcomes. We notice that Text2Video-Zero is slightly faster than our method, due to its sparse instead of dense cross-frame attention. However, as we also observe, for the same reason it underperforms in terms of temporal-consistency among generated frames. We refer the reader to the supplementary material for more qualitative comparison.



Figure 6. **Qualitative comparison on ControlVideo setting:** We show edited video frames using our method, in comparison with ControlVideo [49]. Both methods use depth conditioning. Our method reduces latency by 6 \times with indistinguishable or comparable editing quality.

Component	Tem-con \uparrow	Latency (s) \downarrow	
		Inversion	Generation
Optimized-FateZero	0.966	8.90	10.38
+ Object-Centric 3D ToMe	0.967	9.05	10.54
+ Object-Centric Sampling	0.966	7.59	9.58

Table 3. **Quantitative ablation of our contributions:** Here we consider FateZero [33] benchmark setting. Object-Centric 3D ToMe improves temporal-consistency and fidelity without sacrificing latency (refer Fig. 7 for qualitative comparison). By applying Object-Centric Sampling on top of that, we see further improvements in latency, achieving our fastest generations.

5.3. Analysis

Ablation study We ablate our main contributions within the FateZero base model. Specifically, we illustrate the impact of our proposals in Table 3, where we report Tem-con and latency as metrics, and in Fig. 7. Although off-the-shelf optimizations may grant reasonable speed-ups, we found that for extreme token reduction rates its editing results can suffer from generation artifacts. As the figure clearly shows, the addition of Object-Centric 3D ToMe can easily fix most defects on foreground regions by forcing ToMe to operate on other areas, and such benefit comes without major impact on latency. Finally, Object-Centric Sampling enables significant latency savings performing most diffusion iterations on foreground areas only. Somewhat surprisingly, we observe that Object-Centric Sampling helps the generation of background areas too: this is due to the fact that, as we

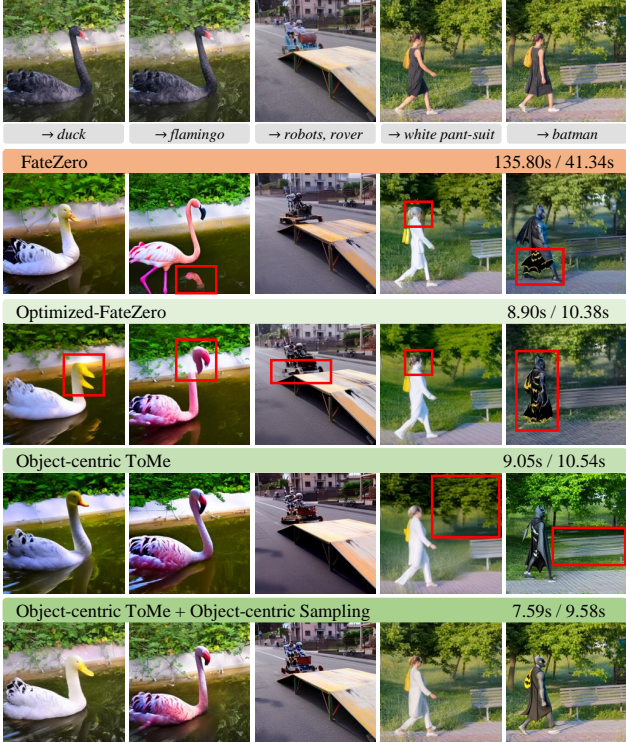


Figure 7. **Qualitative ablation of our contributions:** We show edited frames and latency using Optimized-FateZero, Object-Centric 3D ToMe, and Object-Centric 3D ToMe + Object-Centric Sampling (OCD). We highlight artifacts in generations with red outline. Timings are reported as inversion / generation.

run fewer denoising steps, its representations remain closer to the ones of the original video (resulting from inversion).

Object-Centric Sampling at different object sizes The impact on latency of the proposed Object-Centric Sampling depends on the size of the foreground areas: in the presence of very small edits it can allow significant savings, whereas for prominent objects its editing cost would be only mildly-affected. We study this behavior in Tab. 4, where we divide 18 sequence-prompt pairs in three sets of 6 pairs each, depending on the number of tokens (Δ) within the object bounding box: Large with $\Delta \in [64^2, 48^2]$, Medium with $\Delta \in [48^2, 32^2]$ and Small $\Delta \in [32^2, 0]$. For reference, the number of tokens of a whole frame is 64^2 . As we show in Tab. 4, in the absence of Object-Centric Sampling, the latency of video editing does not depend on the size of the foreground objects. However, although we remark that our proposal reduces latency for all object sizes, we observe that gains are minor on large objects, as the foreground area covers most of the frame resolution and therefore Object-Centric Sampling is more akin to a regular diffusion process operating on the whole frame. Savings are more pronounced for medium and small sized objects, showing additional speed-ups of $1.7\times$ and $2\times$ respectively.

Object size	#tokens (Δ)	w/o Obj-Cen. Sampling			w/ Obj-Cen. Sampling		
		Tem-con \uparrow	Latency (s) \downarrow		Tem-con \uparrow	Latency (s) \downarrow	
			Inv	Gen		Inv	Gen
Large	$[64^2, 48^2]$	0.953	13.04	11.17	0.946	11.80	10.53
Medium	$[48^2, 32^2]$	0.950	12.90	10.83	0.946	7.66	6.72
Small	$[32^2, 0]$	0.979	12.94	10.88	0.975	6.30	5.85

Table 4. **Impact of Object-Centric Sampling at different object sizes.** Here we devise a new benchmark with Large, Medium, and Small foreground objects. We achieve more latency savings with smaller foreground objects without sacrificing the generation quality, while also giving more-faithful background area reconstructions (see last two rows of Fig. 7).

Memory requirement for attention maps As we noted that memory operations are a bottleneck for inversion-based architectures (see Sec. 3), we study the impact of our solutions on the memory required for attention operations. Specifically, we consider FateZero [33], whose attention maps sum up to 74.54 GB of floating point data (16bit). With simple off-the-shelf optimizations, this storage cost is reduced to 5.05 GB, and it can be further lowered to 4.22 GB by applying Object-Centric Sampling. This is a $17\times$ reduction in memory footprint. This finding testifies a lower memory utilization corresponds to a reduced latency, and suggests that our solutions are effective in optimizing them.

Limitations We highlight some potential limitations of our model to be tackled by future work. Although Object-Centric Diffusion represent valuable ideas in general, they are particularly effective for local changes to some peculiar objects, and are slightly less-suitable for global editing (*e.g.* changing the style/textures of a video altogether). Moreover, as most zero-shot methods, in order to achieve the best trade-off between fidelity and latency, our framework still requires to search the best hyperparameters per-sequence.

6. Conclusion

In this paper, we introduced solutions for speeding up diffusion-based video editing. In this respect, we first presented an analysis of sources of latency in inversion-based models, and we identified and adopted some off-the-shelf techniques such as fast sampling and Token Merging that, when properly modified for the task, bring significant cost reduction without sacrificing generation quality. Furthermore, motivated by the fact that video editing typically requires modifications to specific objects, we introduce Object-Centric Diffusion, comprising techniques for *i)* isolating the merging of tokens in background regions only and *ii)* limiting most of the diffusion sampling steps on foreground areas. We validate our solutions on inversion-based and ControlNet-based models, where our strategies achieve $10\times$ and $6\times$ faster editing respectively.

Object-Centric Diffusion for Efficient Video Editing - Supplementary material

A. Additional Discussion

A.1. Off-the-shelf optimizations of ToMe

Pairing token locations from inversion Many inversion-based editing pipelines rely on sharing attention maps between inversion and generation stages (such as FateZero [33] and Plug-and-Play [44]). As such, when applying ToMe [3, 4], it is important that locations of destination (*dst*) and unmerged (*unm*) tokens are paired in the two stages, at the same attention layer and diffusion step. If that is not the case, tokens or attention maps coming from inversion are not compatible with the ones available at generation time. In practice, we compute which tokens to be merged during inversion, and use the same merges on generation attention maps when fusing. We found this strategy to be of primary importance, as testified by Fig. 3 (d-e) in the main paper.

Re-sampling destination tokens per-frame ToMe for stable diffusion [3] samples *dst* tokens randomly. When extending this to multiple frames, we initially sample the same random locations in each frame, finding this strategy to be sub-optimal. Instead, if we re-sample different random locations in each frame (or, in each temporal window in our 3D implementation), it allows us to preserve different information after merging. We found this to be beneficial, especially at higher merging rates (e.g. see Fig. 3 (e to f) in the main paper).

How to search for destination match In the original ToMe for stable diffusion [3], for each source (*src*) token, we search its corresponding match within a pool of *dst* tokens coming from the full spatial extent of the image ($H \times W$). The naive transposition of this strategy to our video use-case allows, for any *src* token, its candidate match to be searched within a pool of *dst* tokens coming from the full spatio-temporal extent of the video ($T \times H \times W$). We find that this strategy for searching *dst* match, named hereby *Temporally-Global Search*, can lead to generation artifacts. Differently, we consider restricting the temporal extent of the *dst* pool to be the same temporal-window ($s_t \times H \times W$) as the *src* token, as in our *Temporally-Windowed Search*. As shown in Fig. A.8, the latter gives better reconstructions in general, whilst allowing more flexibility to control where merges are happening. This way, the user can also better trade-off the temporal-redundancy, smoothness and consistency by controlling the spatio-temporal window size.

Merging queries, keys or values? In our early experiments, we consider applying ToMe to all queries (with un-

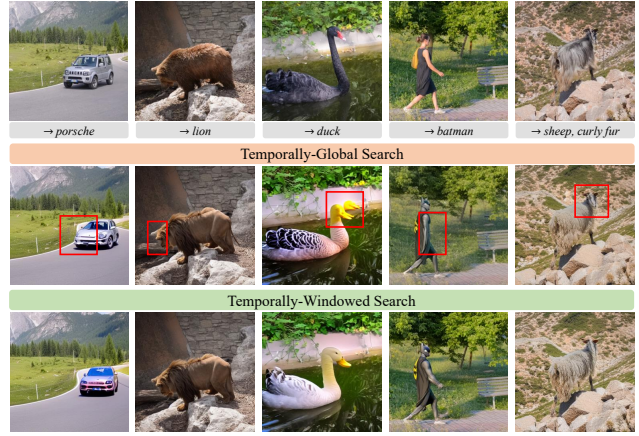


Figure A.8. **Qualitative ablation on searching *dst* match** Each *src* token may search for its corresponding match within a pool of *dst* tokens. This pool can be comprised of either the whole spatio-temporal extent (i.e., all frames) as in *Temporally-Global Search*, or only the same temporal window as the corresponding *src* token as in *Temporally-Windowed Search*. Among these two strategies, the latter allows more flexibility, providing more-consistent generations with better fidelity.

merging, as in [3]), keys and values. We however find that, with extreme reduction rates, merging queries can easily break the reconstructions. As such, we limit ToMe to operate on keys and values only. We also observe that in dense cross-frame attention modules, merging queries only provide a slight latency reduction.

Capped merging in low-res UNet stages As observed in [3], the high resolution UNet [39] stages are the most expensive in terms of self-attention (or, cross-frame attention) modules, and the ones that can benefit the most by applying ToMe. Contrarily to the original formulation which does not optimize low-resolution layers, we do apply ToMe in all layers as we observe it has a meaningful impact on latency. We however cap the minimum #tokens in low-resolution layers in order to avoid degenerate bottlenecks (e.g. collapsing to a single representation). Specifically, we maintain at-least 4 and 16 tokens per-frame after merging at 8×8 and 16×16 resolutions, respectively.

A.2. Benchmark settings

Evaluation metrics We consider two metrics for quantitative evaluation: CLIP-score and Temporal-consistency, similar to prior work [33, 49]. CLIP-score is computed as the cosine similarity between CLIP [35] visual embedding of each frame and CLIP text embedding of the correspond-

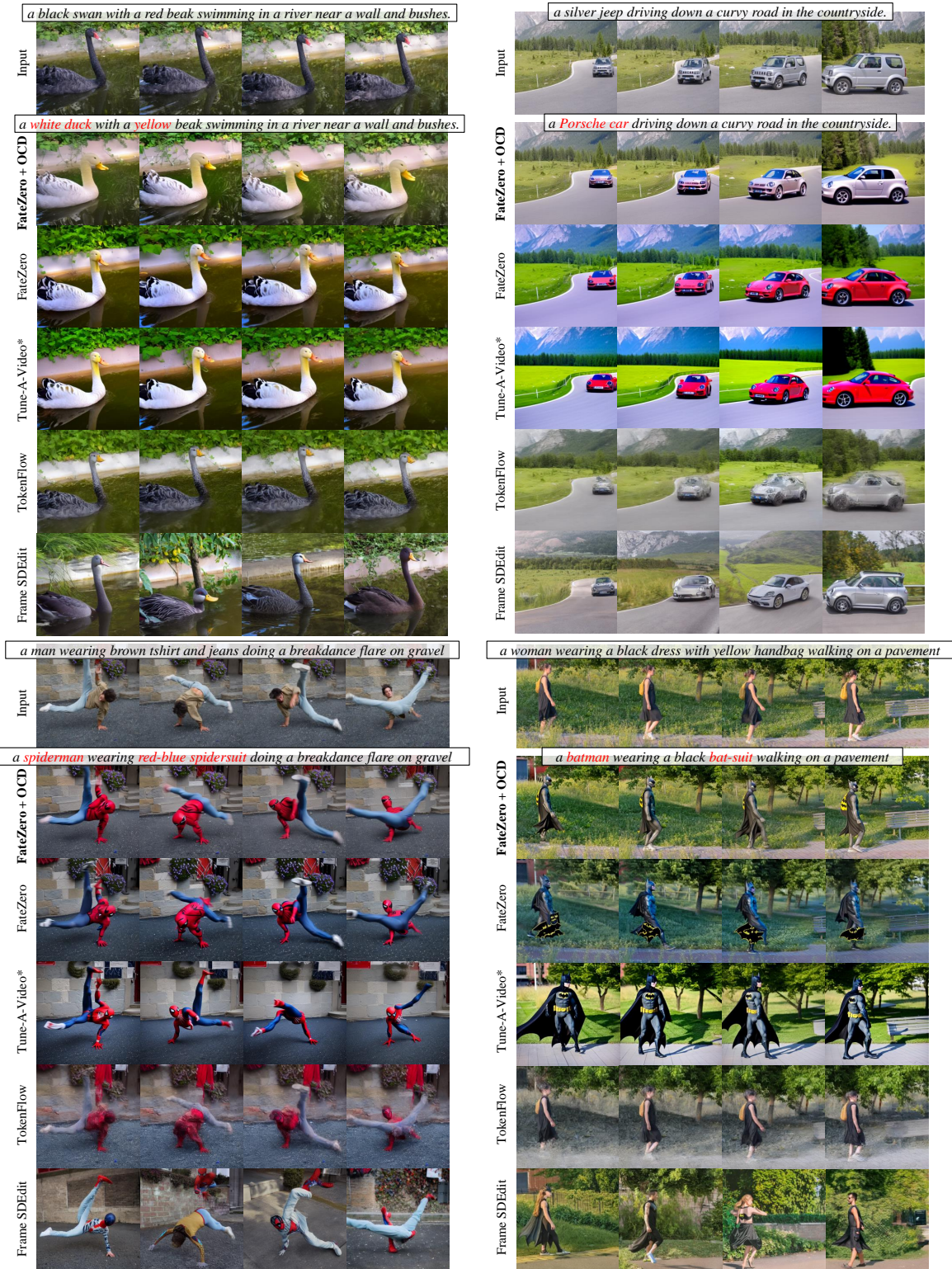


Figure B.1. **Qualitative comparison on *blackswan*, *car-turn*, *breakdance-flare* and *lucia* sequences [32]:** We show shape editing results of our method (Optimized-FateZero + OCD), in comparison with FateZero [33], Tune-A-Video [46], TokenFlow [8] and SDEdit [28]. Our results show better semantic quality (e.g. alignment with target prompt) and visual fidelity (e.g. temporal consistency, faithful background), while also being more efficient (Table 1 in the main paper). Best viewed zoomed-in.

	Sequence	Source prompt	Target prompts
FateZero [33] Benchmark	blackswan	a black swan with a red beak swimming in a river near a wall and bushes.	<ul style="list-style-type: none"> • a white duck with a yellow beak swimming in a river near a wall and bushes. • a pink flamingo with a red beak walking in a river near a wall and bushes. • a Swarovski crystal swan with a red beak swimming in a river near a wall and bushes. • cartoon photo of a black swan with a red beak swimming in a river near a wall and bushes.
	car-turn	a silver jeep driving down a curvy road in the countryside.	<ul style="list-style-type: none"> • a Porsche car driving down a curvy road in the countryside. • watercolor painting of a silver jeep driving down a curvy road in the countryside.
	kite-surf	a man with round helmet surfing on a white wave in blue ocean with a rope.	• a man with round helmet surfing on a white wave in blue ocean with a rope in the Ukiyo-e style painting.
	train (in-the-wild) ¹	a train traveling down tracks next to a forest filled with trees and flowers and a man on the side of the track.	• a train traveling down tracks next to a forest filled with trees and flowers and a man on the side of the track in Makoto Shinkai style.
	rabbit (in-the-wild) ¹	a rabbit is eating a watermelon.	• pokemon cartoon of a rabbit is eating a watermelon.
Large object	breakdance	a man wearing brown tshirt and jeans doing a breakdance flare on gravel.	<ul style="list-style-type: none"> • a woman with long-hair wearing green-sweater and jeans doing a breakdance flare on gravel. • a spiderman wearing red-blue spidersuit doing a breakdance flare on gravel. • a chimpanzee wearing a black jeans doing a breakdance flare on gravel.
	blackswan	a black swan with a red beak swimming in a river near a wall and bushes.	<ul style="list-style-type: none"> • a white duck with a yellow beak swimming in a river near a wall and bushes. • a pink flamingo with a red beak walking in a river near a wall and bushes.
	car-turn	a silver jeep driving down a curvy road in the countryside.	• a Porsche car driving down a curvy road in the countryside.
Medium object	lucia	a woman wearing a black dress with yellow handbag walking on a pavement.	<ul style="list-style-type: none"> • a woman wearing a white pant-suit with yellow handbag walking on a pavement. • a woman wearing a black dress and a hat with red handbag walking on a pavement. • a batman wearing a black bat-suit walking on a pavement.
	bear	a brown bear walking on the rock against a wall.	<ul style="list-style-type: none"> • a red tiger walking on the rock against a wall. • a yellow leopard walking on the rock against a wall.
	blackswan	a black swan with a red beak swimming in a river near a wall and bushes.	• a Swarovski crystal swan with a red beak swimming in a river near a wall and bushes.
Small object	mallard	a brown mallard running on grass land close to a lake.	<ul style="list-style-type: none"> • a white duck running on grass land close to a lake. • a golden chicken running on grass land close to a lake. • a gray goose running on grass land close to a lake.
	boat	a white color metal boat cruising in a lake near coast.	<ul style="list-style-type: none"> • a heavily-rusted metal boat cruising in a lake near coast. • a light-brown color wooden boat cruising in a lake near coast.
	soapbox	two men driving a soapbox over a ramp.	• two robots driving a mars-rover over a ramp.

Table A.5. **Sequence-prompt pairs used to evaluate inversion-based pipelines:** Most sequences here are from DAVIS [32], except for a few in-the-wild videos used in [33]. The Benchmark pairs correspond to the original FateZero [33] quantitative evaluation setting. We also show the sequence-prompt pairs used to evaluate our Object-Centric Sampling, separately for Large, Medium and Small objects. ¹ Videos were downloaded and evaluated on by the first author in their institution.

ing edit prompt, aggregated over all frames and sequences. It measures the semantic fidelity of the generated video. Temporal-consistency is computed as the cosine similarity between the CLIP visual embeddings of each consecutive pairs of frames, aggregated over all pairs and sequences. It conveys the visual quality of the generated video, measuring how temporally coherent frames are. We highlight that, despite their use is due in fair comparisons due to their popularity, both these fidelity metrics are far from perfect. For instance, we find the CLIP score to be sensitive to global semantic discrepancies, yet it often overlooks generation artifacts and smaller pixel-level details. Furthermore, Temporal-Consistency can be simply exploited by a fake video repeating a frame over time. For these reasons, extensive visual comparisons are still required to assess different models, and future research should be encouraged towards more informative quantitative protocols for video editing.

Sequence-prompt pairs We present the sequence-prompt pairs considered in our evaluation of inversion-based pipelines in Table A.5. Most sequences here are from DAVIS [32] dataset, with the exception of a few in-the-wild videos introduced in [33]. The Benchmark setting corresponds to the original quantitative evaluation of FateZero [33], which includes 9 sequence-prompt pairs. We also present the sequence-prompt pairs used to evaluate our Object-Centric Sampling (see Table 4 in the main paper), categorized based on the foreground object size: Large, Medium and Small. Each category includes 6 sequence-prompt pairs. In Table A.2, we show the 125 sequence-prompt pairs used in ControlNet-based pipelines, provided by the authors of ControlVideo [49].

Sequence	Source prompt	Target prompts
blackswan	a black swan moving on the lake.	<ul style="list-style-type: none"> • A black swan moving on the lake • A white swan moving on the lake. • A white swan moving on the lake, cartoon style. • A crochet black swan swims in a pond with rocks and vegetation. • A yellow duck moving on the river, anime style.
boat	a boat moves in the river.	<ul style="list-style-type: none"> • A sleek boat glides effortlessly through the shimmering river, van gogh style. • A majestic boat sails gracefully down the winding river. • A colorful boat drifts leisurely along the peaceful river. • A speedy boat races furiously across the raging river. • A rustic boat bobs gently on the calm and tranquil river.
breakdance-flare	a man dances on the road.	<ul style="list-style-type: none"> • A young man elegantly dances on the deserted road under the starry night sky. • The handsome man dances enthusiastically on the bumpy dirt road, kicking up dust as he moves. • A man gracefully dances on the winding road, surrounded by the picturesque mountain scenery. • The athletic man dances energetically on the long and straight road, his sweat glistening under the bright sun. • The talented man dances flawlessly on the busy city road, attracting a crowd of mesmerized onlookers.
bus	a bus moves on the street.	<ul style="list-style-type: none"> • A big red bus swiftly maneuvers through the crowded city streets. • A sleek silver bus gracefully glides down the busy urban avenue. • A colorful double-decker bus boldly navigates through the bustling downtown district. • A vintage yellow bus leisurely rolls down the narrow suburban road. • A modern electric bus silently travels along the winding coastal highway.
camel	a camel walks on the desert.	<ul style="list-style-type: none"> • A majestic camel gracefully strides across the scorching desert sands. • A lone camel strolls leisurely through the vast, arid expanse of the desert. • A humpbacked camel plods methodically across the barren and unforgiving desert terrain. • A magnificent camel marches stoically through the seemingly endless desert wilderness. • A weathered camel saunters across the sun-scorched dunes of the desert, its gaze fixed on the horizon.
car-roundabout	a jeep turns on a road.	<ul style="list-style-type: none"> • A shiny red jeep smoothly turns on a narrow, winding road in the mountains. • A rusty old jeep suddenly turns on a bumpy, unpaved road in the countryside. • A sleek black jeep swiftly turns on a deserted, dusty road in the desert. • A modified green jeep expertly turns on a steep, rocky road in the forest. • A gigantic yellow jeep slowly turns on a wide, smooth road in the city.
car-shadow	a car moves to a building.	<ul style="list-style-type: none"> • A sleek black car swiftly glides towards a towering skyscraper. • A shiny silver vehicle gracefully maneuvers towards a modern glass building. • A vintage red car leisurely drives towards an abandoned brick edifice. • A luxurious white car elegantly approaches a stately colonial mansion. • A rusty blue car slowly crawls towards a dilapidated concrete structure.
car-turn	a jeep on a forest road.	<ul style="list-style-type: none"> • A shiny silver jeep was maneuvering through the dense forest, kicking up dirt and leaves in its wake. • A dusty old jeep was making its way down the winding forest road, creaking and groaning with each bump and turn. • A sleek black jeep was speeding along the narrow forest road, dodging trees and rocks with ease. • A massive green jeep was lumbering down the rugged forest road, its powerful engine growling as it tackled the steep incline. • A rusty red jeep was bouncing along the bumpy forest road, its tires kicking up mud and gravel as it went.
cows	a cow walks on the grass.	<ul style="list-style-type: none"> • A spotted cow leisurely grazes on the lush, emerald-green grass. • A contented cow ambles across the dewy, verdant pasture. • A brown cow serenely strolls through the sun-kissed, rolling hills. • A beautiful cow saunters through the vibrant, blooming meadow. • A gentle cow leisurely walks on the soft, velvety green grass, enjoying the warm sunshine.
dog	a dog walks on the ground.	<ul style="list-style-type: none"> • A fluffy brown dog leisurely strolls on the grassy field. • A scruffy little dog energetically trots on the sandy beach. • A majestic black dog gracefully paces on the polished marble floor. • A playful spotted dog joyfully skips on the leaf-covered path. • A curious golden dog curiously wanders on the rocky mountain trail.
elephant	an elephant walks on the ground.	<ul style="list-style-type: none"> • A massive elephant strides gracefully across the dusty savannah. • A majestic elephant strolls leisurely along the lush green fields. • A mighty elephant marches steadily through the rugged terrain. • A gentle elephant ambles peacefully through the tranquil forest. • A regal elephant parades elegantly down the bustling city street.

Table A.6. **Sequence-prompt pairs used to evaluate ControlNet-based pipelines:** All sequences are from DAVIS [32]. These pairs correspond to the original ControlVideo [49] quantitative evaluation setting. [continued...]

Sequence	Source prompt	Target prompts
flamingo	a flamingo wanders in the water.	<ul style="list-style-type: none"> • A graceful pink flamingo leisurely wanders in the cool and refreshing water, its slender legs elegantly stepping on the soft sand. • A vibrant flamingo casually wanders in the clear and sparkling water, its majestic wings spread wide in the sunshine. • A charming flamingo gracefully wanders in the calm and serene water, its delicate neck curving into an elegant shape. • A stunning flamingo leisurely wanders in the turquoise and tranquil water, its radiant pink feathers reflecting the shimmering light. • A magnificent flamingo elegantly wanders in the sparkling and crystal-clear water, its striking plumage shining brightly in the sun.
gold-fish	golden fishers swim in the water.	<ul style="list-style-type: none"> • Majestic golden fishers glide gracefully in the crystal-clear waters. • Brilliant golden fishers swim serenely in the shimmering blue depths. • Glittering golden fishers dance playfully in the glistening aquamarine waves. • Gleaming golden fishers float leisurely in the peaceful turquoise pools. • Radiant golden fishers meander lazily in the tranquil emerald streams.
hike	a man hikes on a mountain.	<ul style="list-style-type: none"> • A rugged man is trekking up a steep and rocky mountain trail. • A fit man is leisurely hiking through a lush and verdant forest. • A daring man is scaling a treacherous and jagged peak in the alpine wilderness. • A seasoned man is exploring a remote and rugged canyon deep in the desert. • A determined man is trudging up a snowy and icy mountain slope, braving the biting cold and fierce winds.
hockey	a player is playing hockey on the ground.	<ul style="list-style-type: none"> • A skilled player is furiously playing ice hockey on the smooth, glistening rink. • A young, agile player is energetically playing field hockey on the lush, green grass. • An experienced player is gracefully playing roller hockey on the sleek, polished pavement. • A determined player is passionately playing street hockey on the gritty, urban asphalt. • A talented player is confidently playing air hockey on the fast-paced, neon-lit table.
kite-surf	a man is surfing on the sea.	<ul style="list-style-type: none"> • A muscular man is expertly surfing the gigantic waves of the Pacific Ocean. • A handsome man is gracefully surfing on the crystal clear waters of the Caribbean Sea. • A daring man is fearlessly surfing through the dangerous, choppy waters of the Atlantic Ocean. • An athletic man is skillfully surfing on the wild and untamed waves of the Indian Ocean. • A young man is confidently surfing on the smooth, peaceful waters of a serene lake.
lab-coat	three women stands on the lawn.	<ul style="list-style-type: none"> • Three stunning women are standing elegantly on the lush green lawn, chatting and laughing. • Three young and vibrant women are standing proudly on the well-manicured lawn, enjoying the sunshine. • Three fashionable women in colorful dresses are standing gracefully on the emerald green lawn, taking selfies. • Three confident women with radiant smiles are standing tall on the soft, green lawn, enjoying the fresh air. • Three beautiful women, each dressed in their own unique style, are standing on the lush and verdant lawn, admiring the scenery.
longboard	a man is playing skateboard on the alley.	<ul style="list-style-type: none"> • A young man is skillfully skateboarding on the busy city street, weaving in and out of the crowds with ease. • An experienced skateboarder is fearlessly gliding down a steep, curvy road on his board, executing impressive tricks along the way. • A daring skater is performing gravity-defying flips and spins on his board, effortlessly navigating through a challenging skatepark course. • A talented skateboarder is carving up the smooth pavement of an empty parking lot, creating beautiful patterns with his board and body. • A passionate skater is practicing his moves on a quiet neighborhood street, with the sound of his board echoing through the peaceful surroundings.
mallard-water	a mallard swims on the water.	<ul style="list-style-type: none"> • A vibrant mallard glides gracefully on the shimmering water. • A beautiful mallard paddles through the calm, blue water. • A majestic mallard swims elegantly on the tranquil lake. • A striking mallard floats effortlessly on the sparkling pond. • A colorful mallard glides smoothly on the rippling surface of the water.
mbike-trick	a man riding motorbike.	<ul style="list-style-type: none"> • A young man riding a sleek, black motorbike through the winding mountain roads. • An experienced man effortlessly riding a powerful, red motorbike on the open highway. • A daring man performing gravity-defying stunts on a high-speed, blue motorbike in an empty parking lot. • A confident man cruising on a vintage, yellow motorbike along the picturesque coastal roads. • A rugged man maneuvering a heavy, dusty motorbike through the rugged terrain of a desert.

Table A.2. **Sequence-prompt pairs used to evaluate ControlNet-based pipelines:** All sequences are from DAVIS [32]. These pairs correspond to the original ControlVideo [49] quantitative evaluation setting. [continued...]

Sequence	Source prompt	Target prompts
rhino	a rhino walks on the rocks.	<ul style="list-style-type: none"> • A massive rhino strides confidently across the jagged rocks. • A majestic rhino gracefully navigates the rugged terrain of the rocky landscape. • A powerful rhino marches steadily over the rough and rocky ground. • A colossal rhino plods steadily through the craggy rocks, undeterred by the challenging terrain. • A sturdy rhino confidently traverses the treacherous rocks with ease.
surf	a sailing boat moves on the sea.	<ul style="list-style-type: none"> • A graceful sailing boat glides smoothly over the tranquil sea. • A sleek sailing boat cuts through the shimmering sea with ease. • A majestic sailing boat cruises along the vast, azure sea. • A vintage sailing boat bobs gently on the calm, turquoise sea. • A speedy sailing boat races across the glistening, open sea.
swing	a girl is playing on the swings.	<ul style="list-style-type: none"> • A young girl with pigtails is joyfully swinging on the colorful swings in the playground. • The little girl, giggling uncontrollably, is happily playing on the old-fashioned wooden swings. • A blonde girl with a big smile on her face is energetically playing on the swings in the park. • The girl, wearing a flowery dress, is gracefully swaying back and forth on the swings, enjoying the warm breeze. • A cute little girl, dressed in a red coat, is playfully swinging on the swings, her hair flying in the wind.
tennis	a man is playing tennis.	<ul style="list-style-type: none"> • The skilled man is effortlessly playing tennis on the court. • A focused man is gracefully playing a game of tennis. • A fit and agile man is playing tennis with precision and finesse. • A competitive man is relentlessly playing tennis with his opponent. • The enthusiastic man is eagerly playing a game of tennis, sweat pouring down his face.
walking	a selfie of walking man.	<ul style="list-style-type: none"> • A stylish young man takes a selfie while strutting confidently down the busy city street. • An energetic man captures a selfie mid-walk, showcasing his adventurous spirit. • A happy-go-lucky man snaps a selfie as he leisurely strolls through the park, enjoying the sunny day. • A determined man takes a selfie while briskly walking towards his destination, never breaking stride. • A carefree man captures a selfie while wandering aimlessly through the vibrant cityscape, taking in all the sights and sounds.

Table A.2. **Sequence-prompt pairs used to evaluate ControlNet-based pipelines:** All sequences are from DAVIS [32]. These pairs correspond to the original ControlVideo [49] quantitative evaluation setting.

B. Additional results

B.1. Qualitative comparisons

We show additional qualitative comparisons for inversion-based pipelines in Fig. B.1. Here, we mainly focus on shape editing, and present multiple edited frames of each sequence using FateZero [33], Tune-A-Video [46], TokenFlow [8] and Frame SDEdit [28]. Tune-A-Video requires 1-shot finetuning on a given sequence, whereas TokenFlow and Frame SDEdit are based on stable diffusion [38] checkpoints. FateZero and our implementation rely on Tune-A-Video checkpoints for shape editing, without needing any further finetuning for their respective proposed improvements. Frame SDEdit shows no consistency among frames, being an image editing pipeline. Among video editing pipelines, ours show the best fidelity and temporal-consistency, while also generating outputs faster (see latency measurements given in Table 1 and Fig. 5 in the main paper). Notably, thanks to Object-Centric Sampling, our pipeline gives more-faithful background reconstructions, as such regions are expected to be un-edited based on the given shape editing prompts.

In Fig. B.2, we show additional qualitative comparisons for ControlNet-based pipelines such as ControlVideo [49] and Text2Video-Zero [17]. Here, all methods are conditioned on Depth-maps, while using SD [38] checkpoints without further finetuning. OCD shows comparable per-

Model	CLIP metrics \uparrow		Latency (s) \downarrow		
	Tem-con	Cl-score	Inv	Gen	UNet
FateZero [33]	0.961	0.344	135.80	41.34	20.63
+ diff. steps=5	0.968	0.306	14.84	4.98	2.17
+ diff. steps=20	0.961	0.341	61.82	18.41	8.03
+ avg. pool (4,4)	0.958	0.335	9.91	11.80	7.08
+ max pool (4,4)	0.959	0.275	9.96	11.91	6.91
Optimized-FateZero	0.966	0.334	9.54	10.14	7.79
+ OCD	0.967	0.331	8.22	9.29	6.38

Table B.1. **Additional FateZero [33] baselines:** We report CLIP metrics of fidelity (Temporal-consistency, CLIP-score) and latency (inversion, generation, UNet [39] time). The difference between inversion and UNet time corresponds to other overheads, dominated by memory access. Fewer diffusion steps (*e.g.* 5) and pooling operations can also gain significant speed-ups, but break reconstructions (not always visible in fidelity metrics).

formance with its baseline ControlVideo, while being significantly faster (see latency measurements given in Table 2 in the main paper). It is also more temporally-consistent compared to Text2Video-Zero which uses sparse instead of dense cross-frame attention, while having comparable latency.

B.2. Quantitative comparisons

Other baselines for latency reduction We discuss simple baselines for reducing latency in Table B.1 and Table B.2.

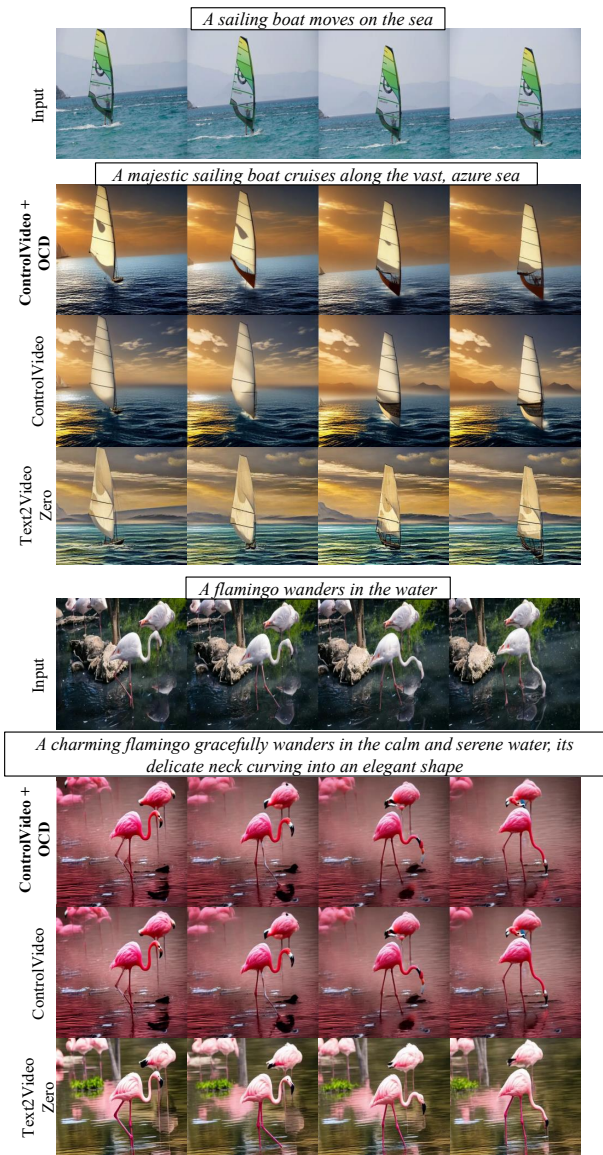


Figure B.2. **Qualitative comparison on surf and flamingo sequences [32]:** We show shape editing results of our method (Optimized-ControlVideo + OCD), in comparison with ControlVideo [49] and Text2Video-Zero [17]. All methods use Depth conditioning. Our results show comparable quality with baseline ControlVideo while being significantly faster (Tab 2 in the main paper), and better temporal consistency compared to Text2Video-Zero. Best viewed zoomed-in.

We report both fidelity (Temporal-consistency, CLIP-score) and latency (inversion, generation, UNet [39] time). Here, UNet time corresponds to just running UNet inference without any additional overheads (*e.g.* memory access), which we use to highlight the cost of such overheads. For ControlVideo [49] baselines, we show results with either Depth or Canny-edge conditioning.

In both inversion-based and ControlNet-based settings, we

Model	CLIP metrics \uparrow		Latency (s) \downarrow	
	Tem-con	Cl-score	Gen	UNet
ControlVideo [49]	0.972 (0.968)	0.318 (0.308)	152.64	137.68
+ diff. steps=5	0.978 (0.971)	0.309 (0.295)	19.58	13.58
+ diff. steps=20	0.978 (0.971)	0.316 (0.304)	64.61	54.83
+ avg.pool (2,2)	0.977 (0.968)	0.309 (0.295)	30.53	20.56
+ max.pool (2,2)	0.972 (0.973)	0.225 (0.212)	30.32	20.53
Optimized-ControlVideo	0.978 (0.972)	0.314 (0.303)	31.12	21.42
+ OCD	0.977 (0.967)	0.313 (0.302)	25.21	15.61
+ OCD (UNet, ControlNet)	0.976 (0.969)	0.306 (0.297)	25.13	15.41
+ ControlNet Red. Inf.	0.977 (0.968)	0.313 (0.301)	23.62	15.47
+ ControlNet Sin. Inf.	0.973 (0.964)	0.307 (0.293)	22.35	15.48

Table B.2. **Additional ControlVideo [49] baselines:** We report CLIP metrics of fidelity (Temporal-consistency, CLIP-score) with either Depth or (Canny-edge) conditioning, and latency (generation, UNet [39] time). The difference between generation and UNet time corresponds to other overheads, dominated by ControlNet [48]. Fewer diffusion steps (*e.g.* 5) and pooling operations can also gain significant speed-ups, but break reconstructions (not always visible in fidelity metrics). We also observe that ControlNet inference need not be done at the same frequency as denoising, which can lead to further speed-ups.

Model	Disk-space (GB) \downarrow
FateZero	74.54
+ diff. steps=5	7.45
+ diff. steps=20	29.82
+ pool (4,4)	3.06
Optimized-FateZero	5.05
+ OCD	4.22

Table B.3. **Memory requirement for attention maps:** In FateZero [33] setting, we show additional baselines and the corresponding storage requirements which directly affect the memory-access overhead. FateZero stores attention maps of all UNet [39] blocks for all diffusion steps. Our contributions help reduce this cost. It can potentially enable attention maps to be kept on GPU memory itself (w/o having to move between GPU and RAM), further improving latency. Each float is stored in 16bits.

devise our optimized-baselines by reducing diffusion steps 50 \rightarrow 20 and applying token merging, which give reasonable reconstructions. This is our default starting point for implementing OCD. Going further, we also consider diff. steps=5, which fails to retain details in reconstructions. Instead of token merging, we can also apply pooling strategies on key-value tokens. Despite giving similar speed-ups, these result in sub-par performance compared to ToMe, especially in shape editing (although not always captured in quantitative numbers). In ControlVideo setup, we can choose to do merging on both UNet and ControlNet [48] models, resulting in further speed-ups with a minimal drop in fidelity. We further observe that we can re-use the same control signal for multiple diffusion steps, allowing us to run ControlNet at a reduced rate (Reduced/Single inference in Table B.2).

Blending steps ratio (γ)	Latency (s) @ #tokens (Δ) ↓							
	64×64		48×48		32×32		16×16	
	Inv	Gen	Inv	Gen	Inv	Gen	Inv	Gen
1.00	12.31	10.39	-	-	-	-	-	-
0.50	-	-	9.56	8.67	9.05	7.60	8.25	7.01
0.25	-	-	8.03	7.94	7.11	6.00	5.90	4.96
0.05	-	-	6.82	7.17	5.85	4.99	4.43	3.80

Table B.4. **Control experiment on Object-Centric Sampling:** We evaluate the latency savings at different *hypothetical* object sizes (Δ) and blending step ratios (γ). The baseline is with $\Delta = 64 \times 64$ and $\gamma = 1.0$ (with total 20 diffusion steps). We can get the most savings at a smaller object size and blending step ratio. It is worth noting that this control experiment does not correspond to actual sequence-prompt pairs, and is just intended to give the reader an idea about expected savings.

Cost of memory access vs. computations Inversion-based editing pipelines rely on guidance from the inversion process during generation (*e.g.* based on latents [44] or attention maps [33]). When running inference, such features need to be stored (which may include additional GPU→RAM transfer), accessed and reused. This cost can be considerable, especially for resource-constrained hardware. This cost measured in latency, is shown in Table B.1, as the difference between inversion and UNet times. Alternatively, it can also be seen as the storage requirement as given in Table B.3. On FateZero [33], we observe that the storage cost is indeed significant, and affects the latency more than the computations. With OCD, we directly reduce the cost for attention computation, storage and access.

Expected savings of Object-Centric Sampling We run a control experiment to observe the expected latency reductions when using our Object-Centric Sampling, at different object sizes (Δ) and Blending step ratios (γ), given in Table B.4. Here, we consider hypothetical inputs, so that we can ablate the settings more-clearly. The baseline sees inputs of size $\Delta = 64 \times 64$, and runs all diffusion steps at full-resolution ($\gamma = 1.0$). In our Object-Centric Sampling, we use $\gamma = 0.25$ by default, whereas Δ depends on objects in a given sequence. As expected, we can obtain the most savings with fewer blending steps and when foreground objects are smaller in size. A user may refer to this guide to get an idea about the expected savings.

References

- [1] Omri Avrahami, Ohad Fried, and Dani Lischinski. Blended latent diffusion. *ACM Transactions on Graphics (TOG)*, 42(4):1–11, 2023. 1
- [2] Andreas Blattmann, Robin Rombach, Huan Ling, Tim Dockhorn, Seung Wook Kim, Sanja Fidler, and Karsten Kreis. Align your latents: High-resolution video synthesis with latent diffusion models. In *Proceedings of the IEEE conference on Computer Vision and Pattern Recognition*, 2023. 1
- [3] Daniel Bolya and Judy Hoffman. Token merging for fast stable diffusion. In *Proceedings of the IEEE conference on Computer Vision and Pattern Recognition*, 2023. 2, 3, 9
- [4] Daniel Bolya, Cheng-Yang Fu, Xiaoliang Dai, Peizhao Zhang, Christoph Feichtenhofer, and Judy Hoffman. Token merging: Your vit but faster. *International Conference on Learning Representations*, 2023. 2, 3, 9
- [5] Weifeng Chen, Jie Wu, Pan Xie, Hefeng Wu, Jiashi Li, Xin Xia, Xuefeng Xiao, and Liang Lin. Control-a-video: Controllable text-to-video generation with diffusion models. *arXiv preprint arXiv:2305.13840*, 2023. 2
- [6] Patrick Esser, Johnathan Chiu, Parmida Atighehchian, Jonathan Granskog, and Anastasis Germanidis. Structure and content-guided video synthesis with diffusion models. In *IEEE International Conference on Computer Vision*, 2023. 2
- [7] Patrick Esser, Johnathan Chiu, Parmida Atighehchian, Jonathan Granskog, and Anastasis Germanidis. Structure and content-guided video synthesis with diffusion models. In *IEEE International Conference on Computer Vision*, 2023. 2
- [8] Michal Geyer, Omer Bar-Tal, Shai Bagon, and Tali Dekel. Tokenflow: Consistent diffusion features for consistent video editing. *arXiv preprint arXiv:2307.10373*, 2023. 2, 3, 6, 7, 10, 14
- [9] Ian Goodfellow, Jean Pouget-Abadie, Mehdi Mirza, Bing Xu, David Warde-Farley, Sherjil Ozair, Aaron Courville, and Yoshua Bengio. Generative adversarial networks. *Communications of the ACM*, 2020. 1
- [10] Amirhossein Habibian, Davide Abati, Taco S Cohen, and Babak Ehteshami Bejnordi. Skip-convolutions for efficient video processing. In *Proceedings of the IEEE conference on Computer Vision and Pattern Recognition*, 2021. 4
- [11] Amir Hertz, Ron Mokady, Jay Tenenbaum, Kfir Aberman, Yael Pritch, and Daniel Cohen-Or. Prompt-to-prompt image editing with cross attention control. *arXiv preprint arXiv:2208.01626*, 2022. 6, 7
- [12] Jonathan Ho, Ajay Jain, and Pieter Abbeel. Denoising diffusion probabilistic models. *Neural Information Processing Systems*, 2020. 1
- [13] Jonathan Ho, William Chan, Chitwan Saharia, Jay Whang, Ruiqi Gao, Alexey Gritsenko, Diederik P Kingma, Ben Poole, Mohammad Norouzi, David J Fleet, et al. Imagen video: High definition video generation with diffusion models. *arXiv preprint arXiv:2210.02303*, 2022. 2
- [14] Jonathan Ho, Chitwan Saharia, William Chan, David J Fleet, Mohammad Norouzi, and Tim Salimans. Cascaded diffusion models for high fidelity image generation. *Journal of Machine Learning Research*, 2022. 1
- [15] Jonathan Ho, Tim Salimans, Alexey Gritsenko, William Chan, Mohammad Norouzi, and David J. Fleet. Video diffusion models, 2022. 2
- [16] Wenyi Hong, Ming Ding, Wendi Zheng, Xinghan Liu, and Jie Tang. Cogvideo: Large-scale pretraining for text-to-video generation via transformers. *International Conference on Learning Representations*, 2023. 2
- [17] Levon Khachatryan, Andranik Movsisyan, Vahram Tadevosyan, Roberto Henschel, Zhangyang Wang, Shant

- Navasardyan, and Humphrey Shi. Text2video-zero: Text-to-image diffusion models are zero-shot video generators. *arXiv preprint arXiv:2303.13439*, 2023. 2, 7, 14, 15
- [18] Bo-Kyeong Kim, Hyoung-Kyu Song, Thibault Castells, and Shinkook Choi. On architectural compression of text-to-image diffusion models. *arXiv preprint arXiv:2305.15798*, 2023. 2
- [19] Dongjun Kim, Chieh-Hsin Lai, Wei-Hsiang Liao, Naoki Murata, Yuhta Takida, Toshimitsu Uesaka, Yutong He, Yuki Mitsufuji, and Stefano Ermon. Consistency trajectory models: Learning probability flow ode trajectory of diffusion. *arXiv preprint arXiv:2310.02279*, 2023. 1
- [20] Diederik P Kingma and Max Welling. Auto-encoding variational bayes. *arXiv preprint arXiv:1312.6114*, 2013. 1
- [21] Alexander Kirillov, Eric Mintun, Nikhila Ravi, Hanzi Mao, Chloe Rolland, Laura Gustafson, Tete Xiao, Spencer Whitehead, Alexander C Berg, Wan-Yen Lo, et al. Segment anything. *arXiv preprint arXiv:2304.02643*, 2023. 4
- [22] Muyang Li, Ji Lin, Chenlin Meng, Stefano Ermon, Song Han, and Jun-Yan Zhu. Efficient spatially sparse inference for conditional gans and diffusion models. *Neural Information Processing Systems*, 2022. 2, 4
- [23] Yanyu Li, Huan Wang, Qing Jin, Ju Hu, Pavlo Chemerys, Yun Fu, Yanzhi Wang, Sergey Tulyakov, and Jian Ren. Snapfusion: Text-to-image diffusion model on mobile devices within two seconds. *arXiv preprint arXiv:2306.00980*, 2023. 2, 4
- [24] Shaoteng Liu, Yuechen Zhang, Wenbo Li, Zhe Lin, and Jiaya Jia. Video-p2p: Video editing with cross-attention control. *arXiv preprint arXiv:2303.04761*, 2023. 2
- [25] Xingchao Liu, Xiwen Zhang, Jianzhu Ma, Jian Peng, and Qiang Liu. InstafLOW: One step is enough for high-quality diffusion-based text-to-image generation. *arXiv preprint arXiv:2309.06380*, 2023. 4
- [26] Cheng Lu, Yuhao Zhou, Fan Bao, Jianfei Chen, Chongxuan Li, and Jun Zhu. Dpm-solver: A fast ode solver for diffusion probabilistic model sampling in around 10 steps. *Neural Information Processing Systems*, 2022. 1, 2, 4
- [27] Cheng Lu, Yuhao Zhou, Fan Bao, Jianfei Chen, Chongxuan Li, and Jun Zhu. Dpm-solver++: Fast solver for guided sampling of diffusion probabilistic models. *arXiv preprint arXiv:2211.01095*, 2022. 1, 2, 3, 4
- [28] Chenlin Meng, Yang Song, Jiaming Song, Jiajun Wu, Jun-Yan Zhu, and Stefano Ermon. Sdedit: Image synthesis and editing with stochastic differential equations. *International Conference on Learning Representations*, 2022. 6, 10, 14
- [29] Chenlin Meng, Robin Rombach, Ruiqi Gao, Diederik Kingma, Stefano Ermon, Jonathan Ho, and Tim Salimans. On distillation of guided diffusion models. In *Proceedings of the IEEE conference on Computer Vision and Pattern Recognition*, 2023. 1, 2
- [30] Microsoft. Microsoft deepspeed. <https://github.com/microsoft/DeepSpeed>. 3
- [31] Ron Mokady, Amir Hertz, Kfir Aberman, Yael Pritch, and Daniel Cohen-Or. Null-text inversion for editing real images using guided diffusion models. In *Proceedings of the IEEE conference on Computer Vision and Pattern Recognition*, 2023. 6, 7
- [32] Jordi Pont-Tuset, Federico Perazzi, Sergi Caelles, Pablo Arbeláez, Alexander Sorkine-Hornung, and Luc Van Gool. The 2017 davis challenge on video object segmentation. *arXiv:1704.00675*, 2017. 5, 10, 11, 12, 13, 14, 15
- [33] Chenyang Qi, Xiaodong Cun, Yong Zhang, Chenyang Lei, Xintao Wang, Ying Shan, and Qifeng Chen. Fatezero: Fusing attentions for zero-shot text-based video editing. *IEEE International Conference on Computer Vision*, 2023. 1, 2, 3, 5, 6, 7, 8, 9, 10, 11, 14, 15, 16
- [34] Xuebin Qin, Zichen Zhang, Chenyang Huang, Masood Dehghan, Osmar R Zaiane, and Martin Jagersand. U2-net: Going deeper with nested u-structure for salient object detection. *Pattern Recognition*, 2020. 4
- [35] Alec Radford, Jong Wook Kim, Chris Hallacy, Aditya Ramesh, Gabriel Goh, Sandhini Agarwal, Girish Sastry, Amanda Askell, Pamela Mishkin, Jack Clark, et al. Learning transferable visual models from natural language supervision. In *International Conference on Machine Learning*, 2021. 9
- [36] René Ranftl, Katrin Lasinger, David Hafner, Konrad Schindler, and Vladlen Koltun. Towards robust monocular depth estimation: Mixing datasets for zero-shot cross-dataset transfer. *IEEE Transactions on Pattern Analysis and Machine Intelligence*, 2020. 7
- [37] Mengye Ren, Andrei Pokrovsky, Bin Yang, and Raquel Urtasun. Sbnnet: Sparse blocks network for fast inference. In *Proceedings of the IEEE conference on Computer Vision and Pattern Recognition*, 2018. 4
- [38] Robin Rombach, Andreas Blattmann, Dominik Lorenz, Patrick Esser, and Björn Ommer. High-resolution image synthesis with latent diffusion models. In *Proceedings of the IEEE conference on Computer Vision and Pattern Recognition*, 2022. 1, 14
- [39] Olaf Ronneberger, Philipp Fischer, and Thomas Brox. U-net: Convolutional networks for biomedical image segmentation. In *International Conference on Medical Image Computing and Computer Assisted Intervention (MICCAI)*, 2015. 4, 9, 14, 15
- [40] Tim Salimans and Jonathan Ho. Progressive distillation for fast sampling of diffusion models. *International Conference on Learning Representations*, 2022. 1, 2, 4
- [41] Christoph Schuhmann, Romain Beaumont, Richard Vencu, Cade Gordon, Ross Wightman, Mehdi Cherti, Theo Coombes, Aarush Katta, Clayton Mullis, Mitchell Wortsman, et al. Laion-5b: An open large-scale dataset for training next generation image-text models. *Neural Information Processing Systems*, 2022. 1
- [42] Uriel Singer, Adam Polyak, Thomas Hayes, Xi Yin, Jie An, Songyang Zhang, Qiyuan Hu, Harry Yang, Oron Ashual, Oran Gafni, et al. Make-a-video: Text-to-video generation without text-video data. *arXiv preprint arXiv:2209.14792*, 2022. 2
- [43] Jiaming Song, Chenlin Meng, and Stefano Ermon. Denoising diffusion implicit models. *International Conference on Learning Representations*, 2021. 1, 2, 3, 4, 6, 7
- [44] Narek Tumanyan, Michal Geyer, Shai Bagon, and Tali Dekel. Plug-and-play diffusion features for text-driven

- image-to-image translation. In *Proceedings of the IEEE conference on Computer Vision and Pattern Recognition*, 2023. [2](#), [3](#), [6](#), [7](#), [9](#), [16](#)
- [45] Thomas Verelst and Tinne Tuytelaars. Dynamic convolutions: Exploiting spatial sparsity for faster inference. In *Proceedings of the IEEE conference on Computer Vision and Pattern Recognition*, 2020. [4](#)
- [46] Jay Zhangjie Wu, Yixiao Ge, Xintao Wang, Stan Weixian Lei, Yuchao Gu, Yufei Shi, Wynne Hsu, Ying Shan, Xiaohu Qie, and Mike Zheng Shou. Tune-a-video: One-shot tuning of image diffusion models for text-to-video generation. In *IEEE International Conference on Computer Vision*, 2023. [1](#), [2](#), [3](#), [6](#), [7](#), [10](#), [14](#)
- [47] Yi Ke Yun and Weisi Lin. Selfreformer: Self-refined network with transformer for salient object detection. *arXiv preprint arXiv:2205.11283*, 2022. [4](#)
- [48] Lvmin Zhang, Anyi Rao, and Maneesh Agrawala. Adding conditional control to text-to-image diffusion models. In *IEEE International Conference on Computer Vision*, 2023. [2](#), [15](#)
- [49] Yabo Zhang, Yuxiang Wei, Dongsheng Jiang, Xiaopeng Zhang, Wangmeng Zuo, and Qi Tian. Controlvideo: Training-free controllable text-to-video generation. *arXiv preprint arXiv:2305.13077*, 2023. [1](#), [2](#), [3](#), [5](#), [7](#), [9](#), [11](#), [12](#), [13](#), [14](#), [15](#)
- [50] Daquan Zhou, Weimin Wang, Hanshu Yan, Weiwei Lv, Yizhe Zhu, and Jiashi Feng. Magicvideo: Efficient video generation with latent diffusion models. *arXiv preprint arXiv:2211.11018*, 2022. [2](#)